*Advanced Materials Research Vol. 59 (2009) pp 288-292*
*online at http://www.scientific.net*


# High heat flux testing of TiC-doped isotropic graphite for plasma facing components

I. López-Galilea[1,a], G. Pintsuk[2,b], C. García-Rosales[1,c] and J. Linke[2,d]

[1]CEIT and Tecnun (University of Navarra), E-20018 San Sebastián, Spain

[2] Forschungszentrum Jülich GmbH, EURATOM Association, D-52425 Jülich, Germany

[a]ilopez@ceit.es, [b]g.pintsuk@fz-juelich.de, [c]cgrosales@ceit.es, [d]j.linke@fz-juelich.de

**Keywords:** Doped Graphite, Thermal Shock Resistance, Plasma Facing Components

**Abstract**. The technical design solution for the future thermonuclear fusion reactor, ITER, must guarantee a reasonable lifetime from a safety and economical point of view. Carbon fibre reinforced carbon (CFC) is envisaged as a corrective material solution for the strike point area of ITER divertor due to its high thermal shock resistance necessary to withstand excessive heat loads during transient thermal loads; in particular plasma disruptions that can deposit energy densities of several ten $MJm^{-2}$ with a typical timescale in the order of milliseconds. In this work, as potential alternative to CFCs new finely dispersed TiC-doped isotropic graphites with high thermal conductivity and mechanical strength, manufactured using synthetic mesophase pitch "AR" as raw material, have been evaluated under typical disruption conditions using an energetic electron beam at the JUDITH facility.

## Introduction

Plasma facing components (PFCs), particularly the strike point area of ITER divertor, will be subjected to intense thermal loads during normal operation (between 5 and 20 $MWm^{-2}$ [1-2]) and to short transient heat fluxes during off-normal plasma scenarios with high deposition of energy density of several tens of $MJm^{-2}$ [3].

Carbon fibre reinforced carbon (CFC) has been proposed as a corrective material solution for the ITER divertor due to its high thermal shock resistance, necessary to withstand excessive heat loads during those off-normal events [1,4,5]. Main drawbacks of carbon-based materials are their chemical erosion under H bombardment from the plasma [6], and their poor radiation resistance. Other disadvantages include high manufacturing difficulties resulting in high cost, long delivery time and large variation in properties [7], as well as the high and continuously increasing tritium retention with fluence [8], representing a serious safety concern. Previous work [9] reveals that TiC-doped isotropic graphite shows significantly improved performance as PFC compared to pure graphite. The addition of small amounts of TiC not only reduces the chemical erosion of carbon, but it also leads to a substantial increase of thermal conductivity and mechanical strength [10] and thus, to an improvement of the thermal shock resistance [9][11]. On the other hand, the deuterium retention behaviour of doped graphite is comparable to that of pyrolytic graphite [12,8], with quasi-saturation at low fluences. These facts let assume that TiC-doped isotropic graphite may be an attractive, low cost plasma-facing material able to compete with present CFC candidate materials.

The aim of this work is the study of thermal shock resistance of newly developed TiC-doped isotropic graphites with high thermal conductivity and mechanical strength under ITER relevant thermal shock loads. For this purpose, a wide test programme - including modelling by numerical methods (FEM) and simulation experiments to determine the material performance under high heat flux - has been established.

## Experimental

**Materials manufacturing.** A synthetic mesophase pitch named AR, supplied by Mitsubishi Gas Chemical, has been used as starting carbon raw material (average particle size (APS) <10 μm.). As

dopant a TiC powder with 130 nm APS has been selected; TiC was added to the carbon raw powder so as to obtain a final graphitic material with ~ 4 at.% of the metal (*AT1* and *AT2* in table 1). Some samples were additionally doped with ~ 0.5 at.% of α-SiC, (APS 20 nm) (*ATS* in table 1), to obtain a further improvement of the thermal conductivity due to the high graphitization degree of the carbon precipitated during the decomposition of SiC [13]. The manufacturing parameters of the whole process and the first results of their influence on some properties have been described in a forthcoming publication [10]. Additionally, an undoped graphite *A* was manufactured as reference material to compare the tests' results.

| Sample Code | Dopant concentration | Density [gcm$^{-3}$] | $P_{Total}$ [Vol%] | $P_{Open}$ [Vol%] | Lc [nm] | $\sigma_f$ [MPa] | K at RT [W/mK] | Weight loss per shot [mg] | Crater depth [μm] |
|---|---|---|---|---|---|---|---|---|---|
| A | None | 1.86 | 17.1 | 16 | 31 | 45 | 70 | 0.88 | - |
| AT1 | 4 at .% Ti | 2.16 | 8.7 | 0 | 45 | 110 | 113 | 0.59 | ~ 11 |
| AT2 | 4 at .% Ti | 1.99 | 14 | 2 | 95±15 | 83±5 | 218 | 0.57 | ~ 12 |
| ATS | 4 at .% Ti + 0.5 at.% Si | 2.08 | 10.7 | ~0 | 55±18 | 92±2 | 195-200 | 0.46 | ~ 7 |

**Table 1.** Some properties of the materials exposed to electron beam thermal loads. The last two columns show parameters measured after the electron beam tests.

**Parameters of electron beam experiments.** The thermal load experiments were performed in the electron beam test facility JUDITH-I at the Research Centre Jülich, Germany [14]. A fast beam scanning (frequencies of beam scan ~ 45 kHz, acceleration voltage = 120 keV) was applied to guarantee a homogeneously loaded area of 4 × 4 mm$^2$. In order to simulate typical ITER disruption conditions, shots with pulse duration (Δt) of 4-5 ms and an absorbed power density ($P_{abs}$) of ~ 2.4 GWm$^{-2}$ (determined by monitoring the absorbed current) were applied. Additionally, for the samples containing both TiC and SiC, the deposited energy density was increased stepwise for a fixed pulse duration of 4-5 ms, to determine the threshold for the onset of brittle destruction (BD), i.e. the conditions for which particle emission starts [15]. All experiments were carried out at room temperature (RT) in vacuum. A CCD camera was used to detect the emission of particles during the thermal load tests (CCD exposure > Δt). A pyrometer and an infrared scanner were used to provide data on the resulting temperatures at the surface ($T_{surf}$). After the tests, the weight change and the erosion depths were measured with a microbalance and with laser profilometry, respectively. Due to insufficient reflectivity of the undoped graphite sample *A*, profilometry was only possible on the doped materials. The microstructure of the loaded surface was observed by optical microscopy and SEM.

## Results and discussion

**Study of thermal shock resistance of *ATS* material.** For the thermal shock resistance study of the samples containing both TiC and SiC, *ATS*, the deposited energy density was increased stepwise from 3 to 14 MJm$^{-2}$ for a fixed pulse duration of ~5 ms. Figure 2 shows the weight loss versus the absorbed energy density. It is not clear to what extent the kind of plateau observed in the energy range 5 to 8 MJm$^{-2}$ reflects the reality; this plateau is also present when the maximum crater depth is plotted versus the absorbed energy. For *ATS*, the material erosion remains negligible below 4 MJm$^{-2}$ (0.8 GWm$^{-2}$, figure 3a) and no dust generation can be detected; above this level the weight loss increases rapidly due to the emission of small and medium carbon particles which appear as faint trajectories (figure 3b and 3c). These loading conditions are associated with non-negligible macroscopic erosion. The absorbed current $I_{abs}$ on the test sample vs. the time are shown in figure 4 at different deposited energy densities. For low beam currents, $I_{abs}$ remains almost constant throughout the full electron beam pulse; however, a sudden drop is observed at the end of the beam pulse which defines the initiation of the particle release. The origin of this drop is diverse: on the one hand thermo-ionic emission from the heated surface is becoming essential at the end of the

pulse; on the other hand charged particles originating from the heated surface and/or from the ablation vapour have strong impact on the measured current $I_{abs}$. When the beam power is increased this current drop occurs earlier; however, it does not affect the energy transfer to the test sample, since the energy of the emitted charged particles is negligible compared to the one of the incident electrons (120 keV) [15-18].

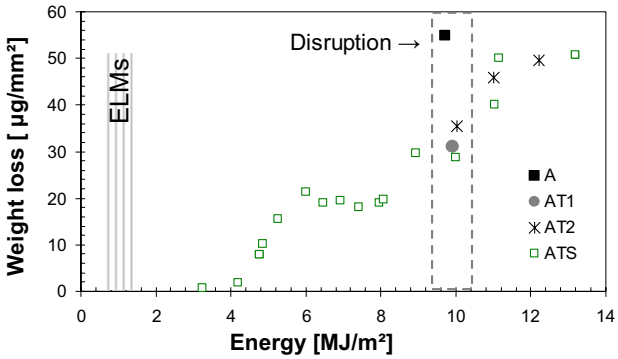


**Figure 2**. Weight loss of different doped and undoped graphites as a function of the absorbed energy density. The energy regions corresponding to ELMs and disruptions are indicated.

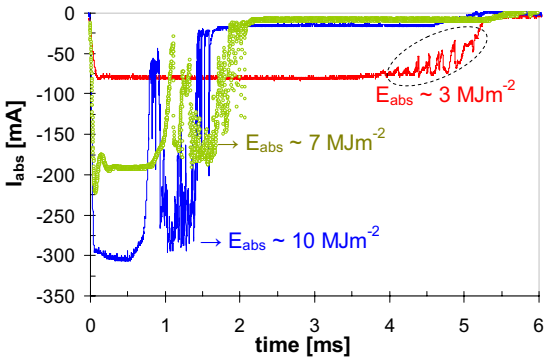


**Figure 4**. Absorbed current for different energy densities deposited on *ATS* samples.

**Figure 3**. Light emission of three ATS samples at different $P_{abs}$ (Δt: 5 ms; loaded area: 4 x 4 $mm^2$).

**a) ATS** ~ 3 $MJm^{-2}$ **b) ATS** ~ 7 $MJm^{-2}$ **c) ATS** ~ 11 $MJm^{-2}$

The high temperatures in the electron beam-exposed surface region result in melting of SiC and TiC, and molten silicon and titanium carbides segregate to the sample surface. The low Si concentration in *ATS* prevents the detection of SiC in the surrounding area of the crater, unlike TiC, detectable at a glance; solidified TiC can be observed as a thin layer over the crater and also in drops ejected from the sample surface in liquid form to the vicinity of the crater (figure 5a). Therefore, it is assumed that at least a significant fraction of the observed particles consists of SiC and TiC droplets, which solidify when coming back to the surface. On the solidified TiC layer there are some superficial cracks (figure 5b) which do not penetrate into the bulk, as confirmed by cross-section analysis (figure 5d). These cracks are located all over the loaded area and increase in number, length and width with increasing power load. In addition, on the upper layer highly ordered graphite is found, due to the strong catalytic effect of molten titanium during the shot, improving as well the thermal conductivity of the surface layer (figure 5c).

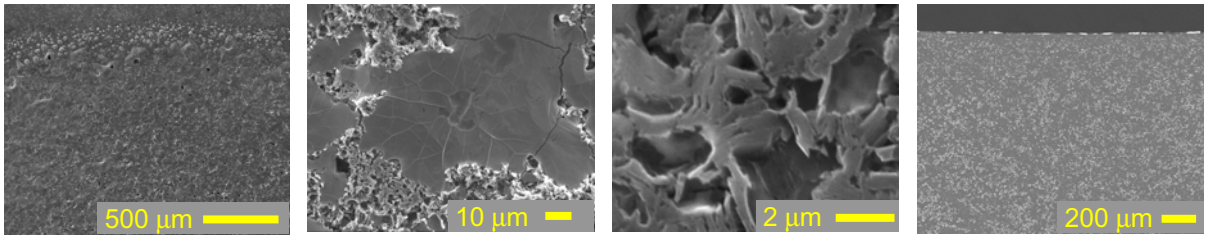


5a) 5b) 5c) 5d)

**Figure 5**: Surface morphology (a, b & c) and cross section (d) of the *ATS* material after electron beam exposure ($E_{abs}$ ~ 10 $MJm^{-2}$; Δt 5 ms).

In order to study the erosion damage by thermal fatigue on the *ATS* material, 10 shots were loaded consecutively. As reported in [9], a slight decrease in particle emission was found when the number of shots is increased (1 versus 10 shots). During the 1st shot, the current plot showed a sudden current spike followed by subsequent spikes probably associated with the emission of dust particles; during the 10th shot however, only a sudden current decrease - which started later in time - was observed. It is assumed that the spikes during the 1st shot can be (at least partly) due to the emission of the small Si amount present in the sample, since no Si at all was detected by EDX after the 1st shot, while a clear Si signal could be measured before the thermal load tests.

**Comparison of different materials under disruption conditions.** The materials listed in table 1 were tested under typical ITER disruption conditions (2.4 $GWm^{-2}$, 4-5 ms corresponding to ~ 10-12 $MJm^{-2}$, see figure 2). As already reported in [9], large and medium dust particles were detected for the undoped graphite *A* during the shot (associated with significant macroscopic erosion). In contrast, a significant reduction of particle emission takes place under the same shot conditions for the Ti-doped graphites, both with Si (*ATS*) and without Si (*AT1* and *AT2*), and only medium and small dust particles were detected. The lower weight loss measured after the shot for these samples is in agreement with this observation. The differences between the doped graphites seem not to be relevant, taking into account the scatter of the data in figure 2. Both weight loss and crater depths are slightly higher for the *AT1* and *AT2* than for the *ATS* sample, even though the particle emission seems to be slightly less for the *AT1* sample [9]. The explanation of these results is not straightforward. Probably the higher thermal conductivity (~200 W/mK at RT) and relatively high flexural strength (~ 92 MPa) of the *ATS* samples could explain their better behaviour (lowest weight loss and crater depth). Surprisingly sample *AT2*, which has the highest thermal conductivity, behaves similar to its homologue in composition *AT1*, probably due to its lower flexural strength.

**Temperature and stress distribution by Finite Element Modelling (FEM).** The internal temperature and stress distributions of the investigated materials during the electron beam tests have been calculated by FEM. Table 2 shows the maximum temperatures and Von Mises stresses ($\sigma_{VM}$) for the different materials at a $P_{abs}$ of 0.4 $GWm^{-2}$ during 5 ms. Under these conditions, the maximum temperature reached on the materials is lower than the melting temperature of TiC (3050 ºC) and the particle emission has not yet started. According to the FEM calculations (figure 6 left), the maximum temperature on the undoped material *A* is analogous to the one of *AT1* due to their similar low thermal conductivity. At first view this result seems to be in disagreement with the experiments (figure 2), where *AT1* has a comparable thermal shock resistance to *AT2* and *ATS* under disruption conditions, and behaves much better than *A*. The explanation of this apparent disagreement is the approximately double strength values ($\sigma_f$) at RT of all doped graphites compared to the undoped one. Assuming only elastic behaviour, and bearing in mind that for C-materials: $\sigma_f$ (1500 ºC) = 1.5×$\sigma_f$ (RT) and $\sigma_f$ (2500 ºC) = 2×$\sigma_f$ (RT) [19], the $\sigma_{VM}$ normalised with the assumed $\sigma_f$ at the corresponding temperature (figure 6 right) explains the large difference between the behaviour of the undoped graphite and all doped graphites, in agreement with the experiment. Values of the normalised stress higher than 1 indicate the possible crack start.

| Sample Code | Max. T [ºC] | Max. Von Mises Stress, $\sigma_{VM}$, [MPa] |
|---|---|---|
| A | 2632 | 289 |
| AT1 | 2585 | 265 |
| AT2 | 2140 | 190 |
| ATS | 2068 | 184 |

$P_{abs}$ of 0.4 $GWm^{-2}$ during 5 ms.

**Table 2**. Max. temperatures and max. *Von Mises* stresses calculated by FEM for the investigated materials.

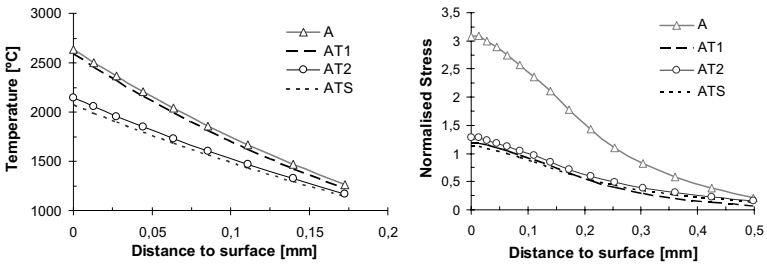


**Figure 6**. (Left) Temperature distribution and (Right) normalised stress for all material, at 0.4 $GWm^{-2}$ during 5 ms, versus the distance to the surface.

## Summary and conclusion

- Dopant addition (Ti and Ti/Si) and a rigorous control of the manufacturing parameters lead to a significant increase of thermal conductivity and mechanical strength compared to pure graphite. This explains that the strong reduction of brittle destruction und high thermal shock loads. No large differences were found between the different TiC-doped graphites under disruption conditions, even though they have significant differences in thermal conductivity. The lower thermal conductivity of one of the doped graphites was compensated by a higher flexural strength. All TiC-doped graphites showed better behaviour than pure graphite.
-The results obtained by FEM using the thermal and mechanical properties of the materials predict the material behaviour under high thermal loads and can be used to forecast the cracking start.

## Acknowledgements

This work has been funded by the European Community within the ExtreMat Integrated Project of the FP6 (NMP3-CT-2004-500253). I. López-Galilea‘s contract is financed by the Ministry of Education of Spain within the framework of Torres Quevedo Programme and co-financed by the European Social Fund. I. López-Galilea gratefully acknowledges the warm reception and hospitality in Forschungszentrum Jülich during her stay there.

## References

[1] H. Bolt V. Barabash, G. Federici, J. Linke, A. Loarte, J. Roth and K. Sato: J. Nucl. Mater. 307–311 (2002), p. 43
[2] R. Aymar and International Team: J. Nucl. Mater. 307-311 (2002), p. 1
[3] J. Linke, T. Hirai, M. Rödig and L. A. Singheiser Fusion Sci. Technol. 46 (2004), p. 142.
[4] V. Barabash, M. Akiba, J.P. Bonal, G. Federici, R. Matera, K. Nakamura, H.D. Pacher, M. Rödig, G. Vieider and C.H. Wu: J. Nucl. Mater. 258–263 (1998), p. 149.
[5] G. Federici G et al.: J. Nucl. Mater. 337–339 (2005), p. 684
[6] J. Roth: Phys. Scr. T124 (2006), p. 37-43.
[7] A. T. Peacock, M. Merola, M. A. Pick and R. Tivey: Phys. Scr. T128 (2007), p. 23-28**.**
[8] J. Roth et al. J. Nucl. Mater. 363-365 (2007), p. 822.
[9] C. García-Rosales, I. López-Galilea, N. Ordás, C. Adelhelm, M. Balden, G. Pintsuk, M. Grattarola and C. Gualco: submitted to Journal of Nuclear materials (2008)
[10] I. López-Galilea, N. Ordás, C. García-Rosales and S. Lindig: submitted to Journal of Nuclear materials (2008)
[11] I. López-Galilea, C. García-Rosales, G. Pintsuk and J. Linke: Phys. Scr. T128 (2007), p. 60
[12] M. Balden, E. Oyarzabal, E. de Juan Pardo, K. Durocher, J. Roth, C. García-Rosales: Phys. Scr. T103 (2003), p 38.
[13] G. Zhang, Q. G. Guo, Z. Liu, L. Yao, L. Liu, J. Li, J. Chen: J. Nucl. Mater. 301 (2002), 187.
[14] R. Duwe, W. Kühnlein, H. Münstermann, in: Proceeding of the 18th SOFT, 1994, p. 355.
[15] J. Linke, S. Amouroux, E. Berthe, Y. Koza, W. Kühnlein, M. Rödig: Fusion Eng. Des. 66–68 (2003), p. 395
[16] J. Linke, M. Akiba, R. Duwe, A. Lodato, H.-J. Penkalla, M. Rödig and K. Schöpflin: J. Nucl. Mater. 290–293 (2001), p. 1102.
[17] J. Linke, H. Bolt, R. Duwe, W. Kühnlein, A. Lodato, M. Rödig, K. Schöpflin and B. Wiechers: J. Nucl. Mater. 283–287 (2000), p. 1152.
[18] J. Linke, R. Duwe, A. Gervash, R.H. Qian, M. Rödig and A Schuster: J. Nucl. Mater. 258–263 (1998), p. 634.
[19] W. Delle, K. Koizlik, H. Nickel: *Graphitische Werkstoffe für den Einsatz in Kernreaktoren. Teil 2*, (Thiemig A. G., Munich, Germany (1983)